Roles of Crystal Surface in Pt-Loaded Titania for Photocatalytic Conversion of Organic Pollutants: A First-Principle Theoretical Calculation

ARTICLE *in* ACS APPLIED MATERIALS & INTERFACES · MAY 2015

Impact Factor: 6.72 · DOI: 10.1021/acsami.5b00079 · Source: PubMed

5 AUTHORS, INCLUDING:

Jie-Jie Chen
University of Science and Technology of China
23 PUBLICATIONS **168** CITATIONS
SEE PROFILE

Wei-Kang Wang
University of Science and Technology of China
7 PUBLICATIONS **40** CITATIONS
SEE PROFILE

Wen-Wei Li
University of Science and Technology of China
162 PUBLICATIONS **1,767** CITATIONS
SEE PROFILE

Han-Qing Yu
University of Science and Technology of China
508 PUBLICATIONS **11,014** CITATIONS
SEE PROFILE

ACS APPLIED MATERIALS & INTERFACES

Research Article

www.acsami.org

Roles of Crystal Surface in Pt-Loaded Titania for Photocatalytic Conversion of Organic Pollutants: A First-Principle Theoretical Calculation

Jie-Jie Chen, Wei-Kang Wang, Wen-Wei Li, Dan-Ni Pei, and Han-Qing Yu*

Department of Chemistry, University of Science & Technology of China, 96 Jingzhai Road, Hefei 230026, China

Supporting Information

ABSTRACT: Titania modified with nanosized metallic clusters is found to substantially enhance its photocatalytic capacity for renewable energy generation and environmental purification, but the underlying mechanism, especially the roles of crystal surface in noble-metal-loaded TiO_2, remain unclear. In this work, such roles in the Pt-loaded anatase TiO_2 for the photocatalytic conversion of nitrobenzene (NB), a model pollutant, are explored by first-principle calculations. The theoretical calculations reveal that the Pt−TiO_2 complex has a higher catalytic activity toward NB conversion than pure Pt clusters, and the (001) facets of TiO_2 in this complex tend to accumulate more positively charged holes and thus have a higher photocatalytic activity than the (101) facets. Furthermore, the thermodynamic and kinetic results also show that the Pt cluster loaded on the (001) surface of anatase TiO_2 is favored for NB conversion in the photooxidation pathway. This work deepens our fundamental understanding on the evolution of molecule−photocatalyst interface and provides implications for designing and preparing photocatalysts.

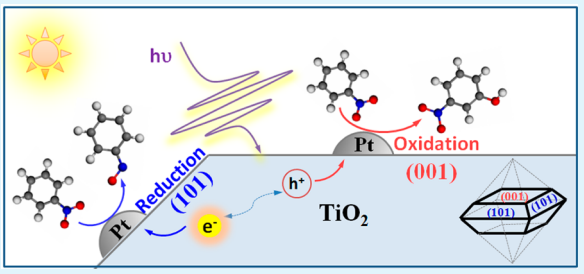

KEYWORDS: *titanium dioxide, photocatalysis, density functional calculations, crystal surface, nitrobenzene, tailored design of catalyst*

INTRODUCTION

Titania with superior physicochemical and optical properties is one of the most widely used benchmark standard photocatalysts in the fields of energy and environment.[1−4] TiO_2 photocatalysis has drawn considerable interests because it offers a possibility for directly utilizing the solar energy and causes no new pollution in energy harvest and water purification.[5−8] Anatase TiO_2 is commonly used as the photocatalyst because of its high photosensitivity and stability, nontoxicity, and good water insolubility.[9−12] However, the photocatalytic degradation efficiency of anatase TiO_2 is usually limited due to the insufficient photocharge generation, resulting from a wide band gap and a rapid recombination of the formed electron−hole pairs.

In order to enhance the generation and separation of electron−hole pairs and accordingly improve its catalytic activity, appropriate engineering of TiO_2 surface properties is usually adopted.[13] Nanostructured clusters of noble metals have been commonly applied as cocatalyst to accelerate the electron−hole separation.[14] For example, loading a small amount of Ag clusters on TiO_2 surface not only drastically increases the photocatalytic activity of TiO_2, but also improves its reaction selectivity toward the reduction of nitrobenzene (NB), as a widely used toxic and environmentally persistent chemical,[15,16] to aniline (AN), a less toxic intermediate.[17,18] Such an improvement is attributed to a strong interfacial bonding between noble-metal cluster and TiO_2 (001) facet, which results in highly delocalized valence electrons of Au[19] and hence accelerated nitroaromatic hydrogenation.[20] A similar enhancement in the adsorption and photocatalytic activity of TiO_2 has been reported by loading a small amount of Pt nanoparticles (NPs) as cocatalyst, demonstrating the high effectiveness of loading metal NPs for enhancing TiO_2 photocatalysis,[21] which is beneficial from a stronger coupling between adsorbate and TiO_2 to accelerate the photogenerated electron transfer.[22]

Although previous studies have shown the high catalytic ability of metal NPs−TiO_2 composite toward the photodegradation of various organic pollutants and identified the decomposition pathways,[15,23] the molecule-level mechanism of metal NPs−TiO_2 composite catalyst remains unclear. Specifically, the molecular configurations of the adsorbed pollutants and intermediates on the catalyst surface, which significantly affect the catalyst−pollutant interactions, are not identified yet. Moreover, other factors governing the photocatalytic performance of such a metal NPs−TiO_2 composite, including the Fermi energy in photostationary state and the solvent properties,[24] also need to be clarified.

The tetra-atomic (M_4) cluster is the simplest three-dimensional system of metal atoms and has been used as a model of highly dispersed catalysts.[25,26] The ultrasmall size of noble-metal clusters is essential for high reactivity.[27] However,

Received: January 5, 2015
Accepted: May 27, 2015
Published: May 27, 2015

DOI: 10.1021/acsami.5b00079
ACS Appl. Mater. Interfaces 2015, 7, 12671−12678

NPs of 2−3 nm diameters containing 200 to 500 atoms are beyond the computational capabilities of density functional theory (DFT).[25] Furthermore, catalytic reactions often occur at the sharp corners, edges, and defect sites of catalyst clusters or surfaces, and these active sites are well-characterized by small subnanoclusters.[28] Thus, a small cluster Pt_4 was used in the calculations to evaluate the effect of the Pt cluster on the catalytic properties. For instance, tetra-atomic transition metal clusters (Fe_4, Co_4, Ni_4, Cu_4, and Pt_4) were used to investigate the electrochemical reduction of CO_2 to CO, HCOOH, and CH_4 by computational methods.[29] A tetrahedral Pt_4 cluster as an initial step was used to understand the oxygen reduction and water splitting reaction path on small Pt NPs or nanoclusters.[25] A small Pd_4 cluster and Pd_nM_{4-n} alloys have been used in the first-principle calculations to explore the catalytic properties.[30,31]

Therefore, this study aims to explore the underlying mechanism and the effective crystal surface of the Pt-cluster-loaded nanocrystalline TiO_2 (Pt/TiO_2) composite catalyst for the primary steps of NB conversion, which has been widely used as a model pollutant to evaluate the photocatalytic activity of designed catalysts.[32,33] To identify the active sites and configurations of the adsorbed NB and intermediate molecules, DFT quantum chemical calculations were applied to calculate the interactions between the reactants (NB, H_3O^+, and $^{\bullet}OH$) and the catalyst surface. DFT-based molecular simulation offers an effective tool to explore molecular-level interactions, identify the configuration changes of nitroaromatic compounds,[34] reveal the origin of the experimentally observed interruption in the periodic arrangement of NB molecules on Si(001) at a molecular-level,[35] and elucidate the roles of protons and water molecules in NB decomposition.[17] DFT calculations can also be used to analyze the influence of the adsorbed ions (F^-, OH^-, and Cl^-) on the interactions between the HCHO molecules and the TiO_2 (001) surface.[36] New photocatalytically active materials with heterostructures of rutile TiO_2 modified with non-transition-metal-oxide nanoclusters can be constructed to predict the photocatalytic behavior through the first-principle calculations.[37] By means of this effective tool, the thermodynamic and kinetic aspects of NB degradation on the (001) and (101) surface of the Pt/TiO_2 catalyst were examined to reveal the structural evolution, the reaction pathways, and the rate-controlling step in this process. In this way, our fundamental understanding on the interaction and evolution mechanisms of organic molecules on Pt cluster-loaded TiO_2 could be deepened, and valuable implications for the design and synthesis of new hybrid photocatalysts could be provided.

MATERIALS AND METHODS

Crystal Surface. Both theoretical and experimental findings have provided evidence that the minority (001) facets of anatase TiO_2 in the equilibrium state are highly reactive for oxidation reactions, while the (101) facet is the most stable and abundant surface for reduction reactions.[9,38] The (101) facet of anatase TiO_2 exhibits a sawtooth-like corrugation with 5- to 6-fold coordinated Ti atoms (Ti-5c, Ti-6c), O-2c, and O-3c on the surface. Each slab of (101) surface contains 18 Ti atoms and 36 O atoms. The supercell of TiO_2 (001) surface with a dimension of 7.55 × 7.55 × 18.83 Å^3 includes a (2 × 2) unit in the surface plane and a vacuum region of ∼15 Å. The (001) faces expose 2-fold coordinated, bridging O atom between two Ti atoms (Ti−O−Ti angle is 156°), together with uncapped, pentacoordinated Ti ions (Ti-5c).[39] The (001) anatase contains four Ti-5c atoms each with O-2c and O-3c on the surface. All the slabs of (001) surface contain 8 Ti atoms and 16 O atoms. The supercell of (101) surface with a dimension of 16.33 × 11.33 × 14.24 Å^3 includes a (3 × 3) unit in the surface plane and a vacuum region of ∼10 Å. Reactants, intermediates, and product molecules could be adsorbed on one side of the slab only.

Theoretical Calculations. First-principles DFT calculations were performed on the basis of the generalized gradient approximation (GGA) with plane-wave basis sets and ultrasoft pseudopotentials,[40] as implemented in the CASTEP module[41] of Materials Studio. The exchange-correlation energy and potential were described self-consistently using the Perdew, Burke, and Ernzerhof (PBE) functional.[42] The *Express* quality setting, which has been widely used to study semiconductors, insulators, and nonmagnetic metals with good accuracy, was employed to attain a compromise between speed and accuracy. Here, the tolerance of the energy was set as 1×10^{-3} eV/cell. This setting is an order of magnitude faster than the *Fine* setting, so that the produced results could be sufficiently accurate for exploratory studies. Brillouin zone integration was performed with variable number of *k*-points generated by Monkhorst−Pack algorithm, depending on the unit cell size and shape.[43] For the $Pt/TiO_2(001)$ supercell (7.55 × 7.55 × 18.83 Å^3), the default value of *k*-point set is 2 × 2 × 1, while for the $Pt/TiO_2(101)$ supercell (16.33 × 11.33 × 14.24 Å^3), the default value of *k*-point set is 1 × 1 × 1. Also, the larger supercells (Supporting Information Figure S1) are used to verify the calculated results, and the details are provided in Supporting Information. Linear synchronous transit (LST)/quadratic synchronous transit (QST) methods[44] were used to search transition state structure and calculate energy barrier.

In order to improve the NB photodegradation efficiency, it is essential to find out the optimal surface structures for both oxidation and reduction reactions. For this purpose, the thermodynamic properties of the catalyst surface were analyzed with DMol^3 module.[45,46] The electron density functional is treated by the GGA with the exchange-correlation function of PBE. Double precision numerical basis sets combined with d-functions (DND) were used to describe the valence electrons. All-electron core treatment was utilized to describe the core electrons.

The binding energy (E_b)[47] was calculated to reveal the interaction affinity between the NB molecule and Pt_4 cluster and TiO_2 surface as well as the location of the NB. Also, the interaction between the TiO_2 and the Pt clusters was further characterized using interaction energy (ΔE_{int}), i.e., the difference between the total energy of the adsorbed system ($E_T(Pt/TiO_2(hkl))$) and the sum of energy for the individual Ti surface ($E_T(TiO_2(hkl))$) and Pt clusters ($E_T(Pt_4)$) as follows:

$$\Delta E_{int} = E_T(Pt/TiO_2(hkl)) - E_T(TiO_2(hkl)) - E_T(Pt_4) \quad (1)$$

RESULTS AND DISCUSSION

Pt_4 Cluster on Anatase TiO_2 Surface. Since the location of metal cluster could affect its interaction with TiO_2, the interaction energy (ΔE_{int}) of the Pt/TiO_2 systems with different Pt_4 cluster locations is calculated (Table 1). The slab models of Pt_4 clusters on anatase (001) and (101) TiO_2 surfaces (Figure 1) are optimized using the DFT method. Several different initial configurations and/or starting locations on the surface are relaxed to determine the most stable geometries.

Table 1. Interaction Energies (ΔE_{int}) and Charge Distribution for Binding Configurations of Pt_4 on Anatase TiO_2 Surface According to Figure 1

system	ΔE_{int} (eV)	Mulliken charge of Pt_4 (e)
$Pt/TiO_2(001)$-1	−6.55	0.57
$Pt/TiO_2(001)$-2	−5.70	0.62
$Pt/TiO_2(101)$-1	−4.37	0.11
$Pt/TiO_2(101)$-2	−2.16	0.10

DOI: 10.1021/acsami.5b00079
ACS Appl. Mater. Interfaces 2015, 7, 12671−12678

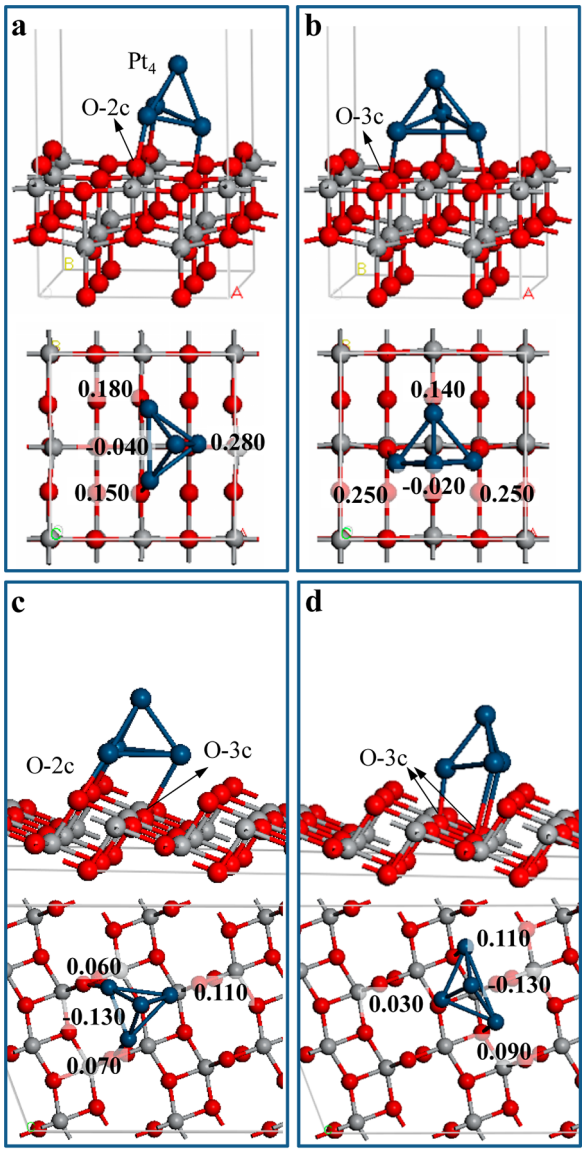

Figure 1. Minimum energy adsorption structure of Pt_4 cluster on (001) and (101) surfaces of the anatase TiO_2 with stereoscopic view and top view, including Mulliken charge of Pt atoms: (a) Pt/TiO_2(001)-1, (b) Pt/TiO_2(001)-2, (c) Pt/TiO_2(101)-1, and (d) Pt/TiO_2(101)-2, Ti atom in light gray, O in red, and Pt in dark blue.

For the Pt/TiO_2(001) system, the preferred location of the Pt_4 cluster (with a lowest ΔE_{int} of −6.55 eV) is that 3 Pt atoms binding to two O-2c sites and one O-3c site of anatase TiO_2 (001) surface (Figure 1a). Likewise, for the Pt/TiO_2(101) system with more stable structure (ΔE_{int} = −4.37 eV), the preferred Pt cluster location is on two O-2c sites and one O-3c site on the (101) surface (Figure 1c). In addition, the Pt cluster loaded on the (001) surface of TiO_2 with more negative values shows a more stable configuration than that on the (101) surface. Apparently, the Pt/TiO_2(001)-1 and Pt/TiO_2(101)-1 models (Figure 1a,c) are appropriate to describe the characteristics of the Pt clusters supported on anatase TiO_2 (001) and (101) surface, respectively. Therefore, the subsequent electronic structures and NB degradation studies are all based on these two Pt/TiO_2 catalyst models.

To determine the charge state of the adsorbed clusters and the interatomic charge distributions, the Mulliken charges, which provide a qualitative measure of the charge redistribution in the system,[48,49] are calculated. The sum of Mulliken charges on all four Pt atoms indicates that the electron density of Pt_4 decreases upon NB adsorption (Table 1). As shown in Figure 1, the three Pt atoms binding directly with the O-2c and O-3c atoms are always positively charged. However, the fourth Pt atom is negatively charged. The Mulliken charge distribution for each Pt atom of Pt_4 cluster on the crystal surface shows a strong covalent characteristic of the bonds formed between Pt and the surface O atoms of TiO_2. Clearly, in all configurations (Figure 1), three Pt atoms become positively charged by losing their electron density upon binding directly with the O-2c and O-3c atoms. As shown by the sum of Mulliken charges (positive values) on all four Pt atoms (Table 1), Pt_4 loses electron density to the surface upon adsorption. Besides, more Mulliken charges are transferred from Pt cluster to the (001) surface than to the (101) surface, indicating that the (001) facets tend to accumulate more positively charged holes and have a higher photooxidative activity than the (101) facets.[50]

Effect of Pt Adsorption on the Electronic Structures of Pt and TiO_2. Since the electrons from Pt atoms can strongly mix with those contributed by Ti and O on the TiO_2 (001) and (101) facets, this electron mixing would undoubtedly affect the electronic structures of both Pt and TiO_2. To substantiate such impacts, we analyze the local density of states (LDOS) plots of the Pt atom and the relevant surface atoms, which illustrate the bonding characteristics. Since the LDOS of O atom is mainly contributed by the p-orbitals, whereas those of Pt and Ti are mainly contributed by the d-orbitals in our energy range of interest, the total LDOS of each atom is used for the calculation in this study. The zero point on the energy axis of the plots corresponds to the Fermi level. As illustrated in Figure 2, the

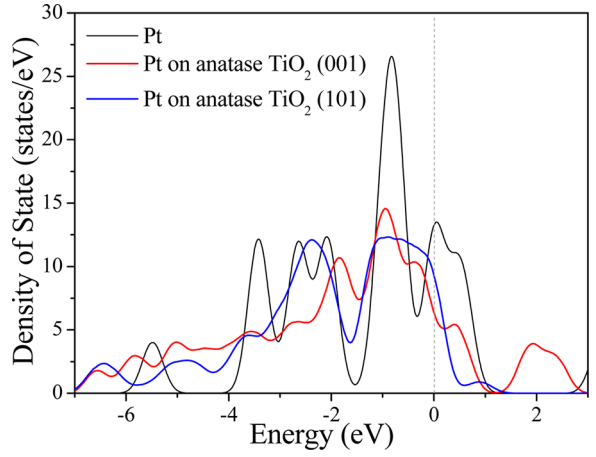

Figure 2. LDOS of Pt in pure Pt cluster and Pt/TiO_2.

LDOSs of a Pt cluster adsorbed on (001) and (101) TiO_2 surfaces are lower than that of pure Pt_4, indicating that the electrons become more unlocalized in the composite system. Additionally, this also implies that the Pt atoms on the TiO_2 surface are more active to react with organic molecules than the pure Pt atoms alone.

Figure 3 shows the LDOS plots of the bare TiO_2 and the Pt/TiO_2 structures. For the configurations of Pt/TiO_2(001)-1 and Pt/TiO_2(101)-1, the metal-induced states of the catalyst band gap are predominantly Pt d-states, although the O states also have a small contribution. The Fermi level pinning can be observed at the heterojunctions of metal−semiconductor

DOI: 10.1021/acsami.5b00079
ACS Appl. Mater. Interfaces 2015, 7, 12671−12678

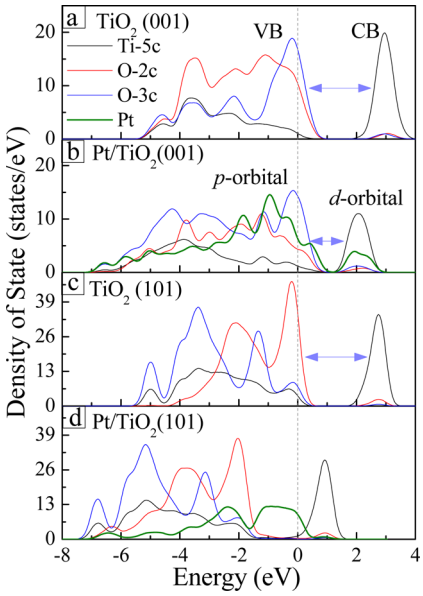

Figure 3. LDOS profiles of surface atoms for (a) bare TiO_2 (001) surface, (b) Pt/TiO_2(001)-1 system, (c) bare TiO_2 (101) surface, (d) and Pt/TiO_2(101)-1 system.

interfaces.[51] Thus, the phenomenon can also be found at the heterojunction of Pt_4 cluster and the anatase TiO_2 surface that the valence band edge is partially pinned to the Pt (Figure 3b). This is consistent with the characteristics of the heterojunctions of Pt_{1-3} and anatase TiO_2 surface, and the small clusters have more obvious behaviors of Fermi level pinning.[48] Moreover, the Fermi level pinning by the noble-metal NPs should extend the lifetime of excitonic electrons, enhancing the charge separation through the noble-metal/semiconductor interfaces.[52]

Additionally, the strong mixing between the Pt d-orbitals and the O p-levels in the Pt/TiO_2(001) system implies that Pt atoms can interact strongly with the O atoms. In contrast, for the Pt/TiO_2(101) system, the whole LDOS moves to the low energy level, accompanied by the formation of high density around the Fermi level and disappearance of the band gap. Due to the strong interfacial bonding, the valence electrons of Pt are highly delocalized in Pt/TiO_2(101).[19]

Thus, these results confirm that the Pt cluster leads to significantly improved NB photodegradation. The metallic units might also enhance the photocatalytic efficiency by promoting charge separation at the metal−semiconductor interfaces.[53] The Pt particles, because of their better electron affinity than TiO_2, could serve as an electron sink to reserve the photogenerated electrons from TiO_2, and hence prevented the electron−hole recombination, and finally promoted the photocatalytic efficiency, and the quantum yield then lowered the overpotential of TiO_2.[53] Among all metal cocatalysts, Pt has been most widely used because of its small work function and low overpotential for solar fuel production.[54,55] This result can be confirmed by the quenching of fluorescence in the photocatalytic systems of noble-metal-loaded TiO_2 as reported previously.[56,57] The photoluminescence emission spectra are used to evaluate the fate of photogenerated electrons and holes in semiconductor as photoluminescence emission results from the recombination of free electrons and holes.[58,59]

Adsorption Configuration of NB on Pt/TiO_2. The configuration of the adsorbed NB on Pt/TiO_2 is obtained through DFT calculations. Figure S2 (Supporting Information) shows the optimized structures of two possible model complexes. In the first model (denoted as NB-Pt), two O atoms of NB are bound to one Pt atom of the Pt_4 cluster (Supporting Information Figure S2a). In the second model (NB-2Pt), two O atoms are separately bound to two Pt atoms (Supporting Information Figure S2b). The optimized structural parameters of the NB−Pt complexes are presented in Supporting Information Table S1. Compared with a free NB molecule, the N−O bond length in the adsorbed configuration is increased from 1.24 to 1.27 Å, but the C−N bond length and the O−N−O bond angle are decreased.

The configuration of NB under stable adsorption state is governed by the binding energy (E_b) of NB with Pt_4. The zero value of E_b represents the situation that a NB molecule is in infinite distance from the Pt cluster. A more negative E_b corresponds to a higher stability of the configuration. The fully optimized structure of the NB−Pt configuration (Supporting Information Figure S2a) has a binding energy of −0.615 eV (Supporting Information Table S2), indicating that this structure is more stable than that of NB−2Pt. Hence, only the NB−Pt configuration is further investigated subsequently.

The charges estimated by the Mulliken population are +0.114 for Pt_4 and −0.260 for NB moieties, indicating that the Pt_4 cluster is electron-donating and NB is electrophilic (Supporting Information Figure S3). This result is consistent with the estimated charges of Ag_4 and NB in a previous study.[17]

According to frontier orbital theory, the highest occupied molecular orbital (HOMO) of Pt (as the electron donor) and the lowest unoccupied molecular orbital (LUMO) of NB (as the electron acceptor) could be the most favorable sites for Pt_4−NB interaction (Supporting Information Figure S4). This means the charge transfer should be from the HOMO of Pt to the LUMO of NB. Therefore, it can be deducted that NB is adsorbed on the Pt_4 cluster with two O atoms of the nitro group. This result is supported by the analysis of the electron density distribution about the attached group on Pt cluster and the binding energy of the stabilization configurations.

The adsorption energy (ΔE_{ad}) of the NB located at the sites of Pt and Ti-5c on (101) surface of Pt/TiO_2(101)-1 was also calculated to clarify the optimal NB adsorption site. Figure 4 shows the energy-minimized geometric structures of proposed adsorption configurations. A more negative ΔE_{ad} corresponds to the favorite site for NB adsorption. The NB on Pt site presents the ΔE_{ad} of −0.913 eV, which is more negative than the NB on Ti-5c site (−0.321 eV) in the Pt/TiO_2(101)-1 system. This is in agreement with the report that a small Pt loading could significantly modify the chemisorption of

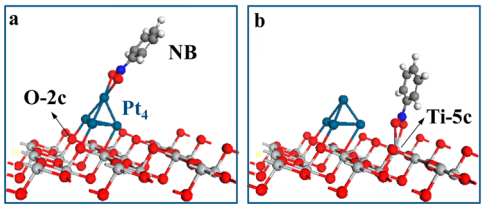

Figure 4. Energy-minimized geometric structures of proposed adsorption configurations of NB located at the sites of (a) Pt and (b) Ti-5c on (101) surface of Pt/TiO_2(101)-1, with Ti atom in light gray, O in red, Pt in dark blue, C in dark gray, H in white, and N in blue.

DOI: 10.1021/acsami.5b00079
ACS Appl. Mater. Interfaces 2015, 7, 12671−12678

TiO_2.[60,61] Therefore, the NB is adsorbed on the Pt site of Pt/TiO_2.

Structural Evolution Mechanism of NB Photocatalytic Conversion on Different Crystal Surfaces of Pt/TiO_2. To better understand the mechanism of NB phototcatalytic conversion on Pt/TiO_2 and structural evolution on different crystal surfaces, these processes are further explored through a series of DFT calculations. It is reported that the (001) facets of anatase TiO_2 are the oxidative sites, whereas the (101) facets are the reductive sites in photocatalytic reactions.[62] In addition, the photocatalytic oxidation of NB conversion is mainly through generating $^{\bullet}OH$ radicals.[63] On the basis of the above analysis, the underlying mechanism of NB conversion on the Pt/TiO_2(001) and Pt/TiO_2(101) surface can be proposed (detailed in Supporting Information Figure S5). In general, the overall process of NB conversion involves a series of oxidation steps on the Pt/TiO_2(001) (eqs 2−5) and reduction steps on the Pt/TiO_2(101) (eqs 6−8). In the reduction process, intermediates including nitrosobenzene (NSB) and hydroxylaminobenzene (HAB) are produced.[15,23]

$$\text{Pt/TiO}_2 + h\nu \rightarrow \text{Pt/TiO}_2\ (e_{CB}^- + h_{VB}^+) \quad (2)$$

$$\text{Pt/TiO}_2(001)(h_{VB}^+) + \text{H}_2\text{O} \rightarrow \text{Pt/TiO}_2(001)(^{\bullet}\text{OH}) + \text{H}^+ \quad (3)$$

$$\text{Pt/TiO}_2(001)\text{-NB} + {}^{\bullet}\text{OH} \rightarrow \text{Pt/TiO}_2(001)\text{-NP} + \text{H}^{\bullet} \quad (4)$$

$$\text{Pt/TiO}_2(001)\text{-NP} + {}^{\bullet}\text{OH} \rightarrow \text{Pt/TiO}_2(001)\text{-NO}_2^{\bullet} + \text{HQ} \quad (5)$$

$$\text{Pt/TiO}_2(101)\text{-NB} + 2\text{H}_3\text{O}^+ + 2(e_{CB}^-) \rightarrow \text{Pt/TiO}_2(101)\text{-NSB} + 3\text{H}_2\text{O} \quad (6)$$

$$\text{Pt/TiO}_2(101)\text{-NSB} + 2\text{H}_3\text{O}^+ + 2(e_{CB}^-) \rightarrow \text{Pt/TiO}_2(101)\text{-HAB} + 2\text{H}_2\text{O} \quad (7)$$

$$\text{Pt/TiO}_2(101)\text{-HAB} + 2\text{H}_3\text{O}^+ + 2(e_{CB}^-) \rightarrow \text{Pt/TiO}_2(101) + \text{AN} + 3\text{H}_2\text{O} \quad (8)$$

Figure 5 depicts the energy-minimized geometric structures of the organic molecules on the Pt/TiO_2 surface. The free energies and the energy barrier (E_a) for both the oxidative and reductive conversion reactions of NB are summarized in Table 2. There is one imaginary frequency for all the transition states (TSs) (Supporting Information Table S3) and no imaginary frequency for the local minima of the primary steps in the oxidation and reduction pathways. Here, the change of Gibbs energy (ΔG) in each elementary step is calculated as

$$\Delta G = \Delta E + \Delta\text{ZPE} - T\Delta S \quad (9)$$

where ΔE is the total energy of system, ΔZPE is the zero-point energy, T is the temperature, and ΔS is the change in entropy. Since the values of ΔZPE and $T\Delta S$ are much smaller than ΔE,[25] their contributions to the free energy can be neglected. Therefore, eq 9 can be approximated as $\Delta G \approx \Delta E$.

The above calculations show that the NB molecule is adsorbed to the Pt/TiO_2 surface at the one Pt site via two O atoms of NO_2 group. The thermodynamic properties of the process for the generation of $^{\bullet}OH$ radicals with the

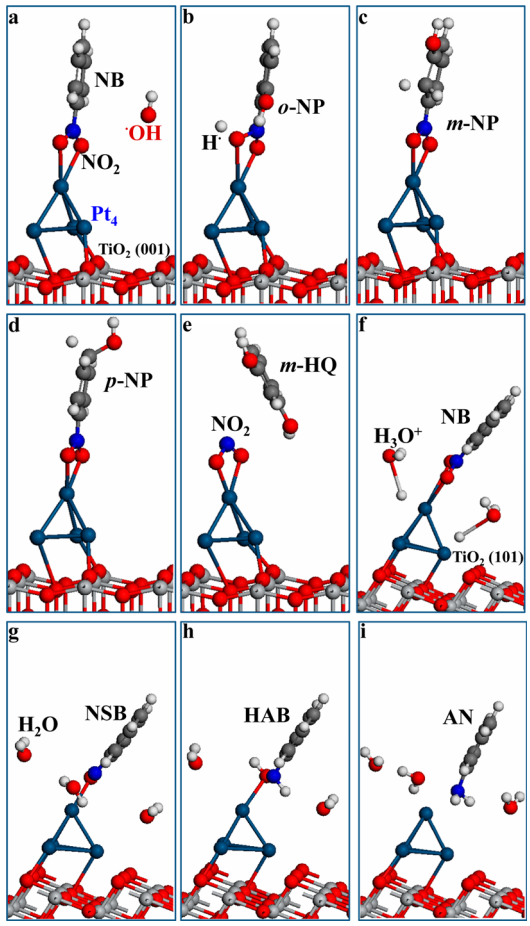

Figure 5. Optimized structures of adsorbed NB and intermediates on Pt/TiO_2 during every step of the NB photoconversion, including (a) Pt/TiO_2(001)-NB, (b) Pt/TiO_2(001)-(o-NP), (c) Pt/TiO_2(001)-(m-NP), (d) Pt/TiO_2(001)-(p-NP), and (e) Pt/TiO_2(001)-$NO_2^{\bullet}$ on Pt/TiO_2(001); and (f) Pt/TiO_2(101)-NB, (g) Pt/TiO_2(101)-NSB, (h) Pt/TiO_2(101)-HAB, and (i) Pt/TiO_2(101) + AN on Pt/TiO_2(101). Colors indicate the following: Ti atom in light gray, O in red, Pt in dark blue, C in dark gray, H in white, and N in blue.

Table 2. Calculated Thermodynamic and Kinetic Properties of the NB Conversion on Pt-Cluster-Loaded (001) and (101) Facets of Anatase TiO_2

step	ΔG (eV)	E_a (eV)
OX-1: Pt/TiO_2(001)-NB + $^{\bullet}$OH → Pt/TiO_2(001)-(*o*-NP) + H$^{\bullet}$	−1.85	0.39
OX-1′: Pt/TiO_2(001)-NB + $^{\bullet}$OH → Pt/TiO_2(001)-(*m*-NP) + H$^{\bullet}$	−2.72	1.85
OX-1″: Pt/TiO_2(001)-NB + $^{\bullet}$OH → Pt/TiO_2(001)-(*p*-NP) + H$^{\bullet}$	−1.89	0.05
OX-2: Pt/TiO_2(001)-(*o*-NP) + $^{\bullet}$OH → Pt/TiO_2(001)-$NO_2^{\bullet}$ + *o*-HQ	−1.99	0.16
OX-2′: Pt/TiO_2(001)-(*m*-NP) + $^{\bullet}$OH → Pt/TiO_2(001)-$NO_2^{\bullet}$ + *m*-HQ	−2.27	1.20
OX-2″: Pt/TiO_2(001)-(*p*-NP) + $^{\bullet}$OH → Pt/TiO_2(001)-$NO_2^{\bullet}$ + *p*-HQ	−3.32	0.43
RED-1: Pt/TiO_2(101)-NB + 2H_3O^+ + 2(e_{CB}^-) → Pt/TiO_2(101)-NSB + 3H_2O	−0.60	2.69
RED-2: Pt/TiO_2(101)-NSB + 2H_3O^+ + 2(e_{CB}^-) → Pt/TiO2(101)-HAB + 2H_2O	−0.10	barrierless
RED-3: Pt/TiO_2(101)-HAB + 2H_3O^+ + 2(e_{CB}^-) → Pt/TiO_2(101) + AN + 3H_2O	−1.02	0.67

DOI: 10.1021/acsami.5b00079
ACS Appl. Mater. Interfaces 2015, 7, 12671−12678

photogenerated holes (h_{VB}^+) were also taken into considerations. In the photocatalytic process, the ΔG value of the elementary step involving proton and hole should deduct the energy ($|e|U$) of electron−hole pair generation. U is the electropotential of a hole (h_{VB}^+) with respect to standard hydrogen electrode (SHE, $U = 0$, $\Delta G_H = 0$), and thus, $|e|U$ represents the energy required to generate the electron−hole pair. Thus, the ΔG values for the generation of •OH radicals on (001) surface of TiO_2 were provided in Supporting Information. Then, in the oxidative conversion of NB, the •OH mainly attacks the adsorbed NB on the ortho-, meta-, and para-sites of benzene relative to the NO_2 group (with ΔG of −1.85, −2.72, and −1.89 eV, respectively), forming adsorbed nitrophenol (Pt/TiO_2(001)-NP, Figure 5b−d). The •OH can be generated from the indirect oxidization of the adsorbed water molecules or from the hydroxyl groups at the positive holes (h_{VB}^+) formed on the valence band (VB). Besides, •OH can also react on the C site that links the NO_2 group, resulting in splitting of the C−N bond and formation of the ortho-, meta-, and para-hydroquinone (HQ) (meta-HQ, Figure 5e).

For the reductive conversion route, the NB on the Pt/TiO_2(101) surface reacts with two H_3O^+ coupled with photogenerated electrons (e_{CB}^-), yielding Pt/TiO_2(101)-NSB (Figure 5g) and three H_2O molecules. The ΔG and E_a values of this process are −0.60 and of 2.69 eV, respectively (Table 2), which are higher than the values of the first step of oxidation pathway (eq 5). Thus, the initial step of the oxidative conversion pathway (OX-1, OX-1′, and OX-1″) is thermodynamically amd kinetically more favorable than the reduction route (RED-1). The Pt cluster only deposited on the (101) surface might have no significant effect on the improvement of NB conversion. Apparently, for the photocatalytic conversion of NB, enhanced generation of h_{VB}^+ for oxidative conversion is favored with a higher initial reaction rate.

The higher photocatalytic activity of the (001) surface in NB conversion is consistent with the experimental observation of photodegradation of methyl orange, in which (001)-TiO_2 has a higher photocatalytic activity than (010)- and (101)-TiO_2.[64] Moreover, the first-principles studies also indicate that the adsorption of gold on TiO_2 (001) is much stronger than that on the (101) surface.[19] In addition, TiO_2/graphene composites have a higher photocatalytic activity compared with the P25 under UV light due to the effective exposure of highly reactive (001) surface.[65] Thus, the validity of the phtotocatalyst model for pollutant degradation can be confirmed, and the results in this work indicate that the NB conversion pathway in the Pt/TiO_2 system is favored through the photooxidation pathway on the (001) surface. Therefore, noble-metal NPs loaded on this facet would enhance the photocatalytic activity to achieve a high efficiency of environmental remediation and energy conversion.

CONCLUSIONS

The roles of (001) and (101) surfaces of Pt/TiO_2 on NB photoconversion in aqueous phase are elucidated by first-principle theoretical calculations. The NB molecules are found to be adsorbed on the catalyst surface at the one Pt site via two O atoms of NO_2 group. The electrons of Pt on anatase TiO_2 (001) and (101) surfaces are more unlocalized than those of pure Pt clusters, which are responsible for the higher catalytic activity of the Pt-TiO_2 complex toward NB coversion. The most rapid NB conversion is achieved over the Pt/TiO_2 catalyst on the (001) surface, indicating that an oxidative conversion route is favored in this system. Thus, the efficiency of NB conversion in aqueous solution could be enhanced by exposing a large ratio of the (001) surface in the synthesis of Pt/TiO_2. Our work offers a molecular-level insight into the structural evolution of organic−inorganic interfaces in NB photoconversion, and provides useful information for guiding a tailored design and fabrication of photocatalysts for photodecomposition implementations.

ASSOCIATED CONTENT

Supporting Information

Details of calculated structural parameters and binding energies of NB-Pt complexes, proposed adsorption configurations of NB on Pt_4 cluster, charge distribution of NB-Pt adsorption configuration, frontier molecular orbital scheme of NB-Pt, and suggested mechanism of the NB conversion on different crystal surface of Pt/TiO_2. The Supporting Information is available free of charge on the ACS Publications website at DOI: 10.1021/acsami.5b00079.

AUTHOR INFORMATION

Corresponding Author

*E-mail: hqyu@ustc.edu.cn.

Author Contributions

J.-J.C. and W.-K.W. contributed equally.

Notes

The authors declare no competing financial interest.

ACKNOWLEDGMENTS

The authors wish to thank the National Basic Research Program of China (2011CB933702), the Program for Changjiang Scholars and Innovative Research Team in University, and the Collaborative Innovation Center of Suzhou Nano Science and Technology of Ministry of Education of China, and the China Postdoctoral Science Foundation (2014M560522) for the partial support of this work. The numerical calculations were performed on the supercomputing system in the Supercomputing Center at the University of Science and Technology of China, China.

REFERENCES

(1) Tachikawa, T.; Majima, T. Metal Oxide Mesocrystals with Tailored Structures and Properties for Energy Conversion and Storage Applications. *NPG Asia Mater.* **2014**, *6*, e100.

(2) Lang, X.; Ma, W.; Chen, C.; Ji, H.; Zhao, J. Selective Aerobic Oxidation Mediated by TiO_2 Photocatalysis. *Acc. Chem. Res.* **2013**, *47*, 355−363.

(3) Wang, M. Y.; Ioccozia, J.; Sun, L.; Lin, C. J.; Lin, Z. Q. Inorganic-Modified Semiconductor TiO_2 Nanotube Arrays for Photocatalysis. *Energy Environ. Sci.* **2014**, *7*, 2182−2202.

(4) Wu, T. T.; Xie, Y. P.; Yin, L. C.; Liu, G.; Cheng, H. M. Switching Photocatalytic H_2 and O_2 Generation Preferences of Rutile TiO_2 Microspheres with Dominant Reactive Facets by Boron Doping. *J. Phys. Chem. C* **2015**, *119*, 84−89.

(5) Chen, C. C.; Ma, W. H.; Zhao, J. C. Semiconductor-Mediated Photodegradation of Pollutants under Visible-Light Irradiation. *Chem. Soc. Rev.* **2010**, *39*, 4206−4219.

(6) Fujishima, A.; Honda, K. Electrochemical Photolysis of Water at a Semiconductor Electrode. *Nature* **1972**, *238*, 37−38.

(7) Mou, Z. G.; Wu, Y. J.; Sun, J. H.; Yang, P.; Du, Y. K.; Lu, C. TiO_2 Nanoparticles-Functionalized N-Doped Graphene with Superior Interfacial Contact and Enhanced Charge Separation for Photocatalytic Hydrogen Generation. *ACS Appl. Mater. Interfaces* **2014**, *6*, 13798−13806.

DOI: 10.1021/acsami.5b00079
ACS Appl. Mater. Interfaces 2015, 7, 12671−12678

(8) Jiang, Y.; Wang, W. N.; Biswas, P.; Fortner, J. D. Facile Aerosol Synthesis and Characterization of Ternary Crumpled Graphene-TiO_2-Magnetite Nanocomposites for Advanced Water Treatment. *ACS Appl. Mater. Interfaces* **2014**, *6*, 11766−11774.
(9) Yang, H. G.; Sun, C. H.; Qiao, S. Z.; Zou, J.; Liu, G.; Smith, S. C.; Cheng, H. M.; Lu, G. Q. Anatase TiO_2 Single Crystals with a Large Percentage of Reactive Facets. *Nature* **2008**, *453*, 638−641.
(10) Yuan, S. J.; Chen, J. J.; Lin, Z. Q.; Li, W. W.; Sheng, G. P.; Yu, H. Q. Nitrate Formation from Atmospheric Nitrogen and Oxygen Photocatalysed by Nano-Sized Titanium Dioxide. *Nat. Commun.* **2013**, *4*, 2249.
(11) Anandan, S.; Rao, T. N.; Sathish, M.; Rangappa, D.; Honma, I.; Miyauchi, M. Superhydrophilic Graphene-Loaded TiO_2 Thin Film for Self-Cleaning Applications. *ACS Appl. Mater. Interfaces* **2013**, *5*, 207−212.
(12) Liu, G.; Yang, H. G.; Wang, X. W.; Cheng, L. N.; Lu, H. F.; Wang, L. Z.; Lu, G. Q.; Cheng, H. M. Enhanced Photoactivity of Oxygen-Deficient Anatase TiO_2 Sheets with Dominant {001} Facets. *J. Phys. Chem. C* **2009**, *113*, 21784−21788.
(13) Hanson, K.; Losego, M. D.; Kalanyan, B.; Ashford, D. L.; Parsons, G. N.; Meyer, T. J. Stabilization of [Ru(Bpy)(2)(4,4′-(PO_3H_2)Bpy)](2+) on Mesoporous TiO_2 with Atomic Layer Deposition of Al_2O_3. *Chem. Mater.* **2013**, *25*, 3−5.
(14) Liu, R.; Sen, A. Controlled Synthesis of Heterogeneous Metal-Titania Nanostructures and Their Applications. *J. Am. Chem. Soc.* **2012**, *134*, 17505−17512.
(15) Wang, A. J.; Cheng, H. Y.; Liang, B.; Ren, N. Q.; Cui, D.; Lin, N.; Kim, B. H.; Rabaey, K. Efficient Reduction of Nitrobenzene to Aniline with a Biocatalyzed Cathode. *Environ. Sci. Technol.* **2011**, *45*, 10186−10193.
(16) Zhang, S. J.; Jiang, H.; Li, M. J.; Yu, H. Q.; Yin, H.; Li, Q. R. Kinetics and Mechanisms of Radiolytic Degradation of Nitrobenzene in Aqueous Solutions. *Environ. Sci. Technol.* **2007**, *41*, 1977−1982.
(17) Tada, H.; Ishida, T.; Takao, A.; Ito, S.; Mukhopadhyay, S.; Akita, T.; Tanaka, K.; Kobayashi, H. Kinetic and DFT Studies on the Ag/TiO_2-Photocatalyzed Selective Reduction of Nitrobenzene to Aniline. *ChemPhysChem* **2005**, *6*, 1537−1543.
(18) Kamegawa, T.; Seto, H.; Matsuura, S.; Yamashita, H. Preparation of Hydroxynaphthalene-Modified TiO_2 via Formation of Surface Complexes and Their Applications in the Photocatalytic Reduction of Nitrobenzene under Visible-Light Irradiation. *ACS Appl. Mater. Interfaces* **2012**, *4*, 6635−6639.
(19) Sun, C.; Smith, S. C. Strong Interaction between Gold and Anatase TiO_2(001) Predicted by First Principle Studies. *J. Phys. Chem. C* **2012**, *116*, 3524−3531.
(20) Cardenas-Lizana, F.; Gomez-Quero, S.; Idriss, H.; Keane, M. A. Gold Particle Size Effects in the Gas-Phase Hydrogenation of M-Dinitrobenzene over Au/TiO_2. *J. Catal.* **2009**, *268*, 223−234.
(21) Kamegawa, T.; Matsuura, S.; Seto, H.; Yamashita, H. A Visible-Light-Harvesting Assembly with a Sulfocalixarene Linker between Dyes and a Pt-TiO_2 Photocatalyst. *Angew. Chem., Int. Ed.* **2013**, *52*, 916−919.
(22) Kim, J.; Monllor-Satoca, D.; Choi, W. Simultaneous Production of Hydrogen with the Degradation of Organic Pollutants Using TiO_2 Photocatalyst Modified with Dual Surface Components. *Energy Environ. Sci.* **2012**, *5*, 7647−7656.
(23) Li, Y. P.; Cao, H. B.; Liu, C. M.; Zhang, Y. Electrochemical Reduction of Nitrobenzene at Carbon Nanotube Electrode. *J. Hazard. Mater.* **2007**, *148*, 158−163.
(24) Tada, H.; Kiyonaga, T.; Naya, S. Rational Design and Applications of Highly Efficient Reaction Systems Photocatalyzed by Noble Metal Nanoparticle-Loaded Titanium(IV) Dioxide. *Chem. Soc. Rev.* **2009**, *38*, 1849−1858.
(25) Roudgar, A.; Eikerling, M.; van Santen, R. *Ab Initio* Study of Oxygen Reduction Mechanism at Pt_4 Cluster. *Phys. Chem. Chem. Phys.* **2010**, *12*, 614−620.
(26) Parreira, R. L. T.; Caramori, G. F.; Galembeck, S. r. E.; Huguenin, F. The Nature of the Interactions between Pt_4 Cluster and the Adsorbates $^{\bullet}H$, $^{\bullet}OH$, and H_2O. *J. Phys. Chem. A* **2008**, *112*, 11731−11743.
(27) Liu, Z. P.; Jenkins, S. J.; King, D. A. Origin and Activity of Oxidized Gold in Water-Gas-Shift Catalysis. *Phys. Rev. Lett.* **2005**, *94*, 196102.
(28) Dhilip Kumar, T. J.; Zhou, C.; Cheng, H.; Forrey, R. C.; Balakrishnan, N. Effect of Co Doping on Catalytic Activity of Small Pt Clusters. *J. Chem. Phys.* **2008**, *128*, 124704.
(29) Liu, C.; He, H.; Zapol, P.; Curtiss, L. A. Computational Studies of Electrochemical CO_2 Reduction on Subnanometer Transition Metal Clusters. *Phys. Chem. Chem. Phys.* **2014**, *16*, 26584−26599.
(30) Kalita, B.; Deka, R. C. Reaction Intermediates of CO Oxidation on Gas Phase Pd_4 Clusters: A Density Functional Study. *J. Am. Chem. Soc.* **2009**, *131*, 13252−13254.
(31) Heard, C. J.; Heiles, S.; Vajda, S.; Johnston, R. L. Pd_nAg(4-N) and Pd_nPt(4-N) Clusters on MgO (100): A Density Functional Surface Genetic Algorithm Investigation. *Nanoscale* **2014**, *6*, 11777−11788.
(32) Surolia, P. K.; Tayade, R. J.; Jasra, R. V. Photocatalytic Degradation of Nitrobenzene in an Aqueous System by Transition-Metal-Exchanged ETS-10 Zeolites. *Ind. Eng. Chem. Res.* **2010**, *49*, 3961−3966.
(33) Wahab, H. S.; Koutselos, A. D. Computational Modeling of the Adsorption and (*)OH Initiated Photochemical and Photocatalytic Primary Oxidation of Nitrobenzene. *J. Mol. Model.* **2009**, *15*, 1237−1244.
(34) Norskov, J. K.; Bligaard, T.; Rossmeisl, J.; Christensen, C. H. Towards the Computational Design of Solid Catalysts. *Nat. Chem.* **2009**, *1*, 37−46.
(35) Peng, G. W.; Seo, S.; Ruther, R. E.; Hamers, R. J.; Mavrikakis, M.; Evans, P. G. Molecular-Scale Structure of a Nitrobenzene Monolayer on Si(001). *J. Phys. Chem. C* **2011**, *115*, 3011−3017.
(36) Zhou, P.; Zhu, X. F.; Yu, J. G.; Xiao, W. Effects of Adsorbed F, OH, and Cl Ions on Formaldehyde Adsorption Performance and Mechanism of Anatase Tio_2 Nanosheets with Exposed {001} Facets. *ACS Appl. Mater. Interfaces* **2013**, *5*, 8165−8172.
(37) Nolan, M. First-Principles Prediction of New Photocatalyst Materials with Visible-Light Absorption and Improved Charge Separation: Surface Modification of Rutile TiO_2 with Nanoclusters of MgO and Ga_2O_3. *ACS Appl. Mater. Interfaces* **2012**, *4*, 5863−5871.
(38) Gong, X. Q.; Selloni, A. Reactivity of Anatase TiO_2 Nanoparticles: The Role of the Minority (001) Surface. *J. Phys. Chem. B* **2005**, *109*, 19560−19562.
(39) Hussain, A. A Computational Study of Catalysis by Gold in Applications of CO Oxidation. Ph.D. Thesis, Technische Universiteit Eindhoven, Eindhoven, 2010.
(40) Vanderbilt, D. Soft Self-Consistent Pseudopotentials in a Generalized Eigenvalue Formalism. *Phys. Rev. B* **1990**, *41*, 7892−7895.
(41) Segall, M. D.; Lindan, P. J. D.; Probert, M. J.; Pickard, C. J.; Hasnip, P. J.; Clark, S. J.; Payne, M. C. First-Principles Simulation: Ideas, Illustrations and the Castep Code. *J. Phys.: Condens. Matter* **2002**, *14*, 2717−2744.
(42) Perdew, J. P.; Burke, K.; Ernzerhof, M. Generalized Gradient Approximation Made Simple. *Phys. Rev. Lett.* **1996**, *77*, 3865−3868.
(43) Monkhorst, H. J.; Pack, J. D. Special Points for Brillouin-Zone Integrations. *Phys. Rev. B* **1976**, *13*, 5188−5192.
(44) Halgren, T. A.; Lipscomb, W. N. The Synchronous-Transit Method for Determining Reaction Pathways and Locating Molecular Transition States. *Chem. Phys. Lett.* **1977**, *49*, 225−232.
(45) Delley, B. Fast Calculation of Electrostatics in Crystals and Large Molecules. *J. Phys. Chem.* **1996**, *100*, 6107−6110.
(46) Delley, B. From Molecules to Solids with the $DMol^3$ Approach. *J. Chem. Phys.* **2000**, *113*, 7756−7764.
(47) Vayssilov, G. N.; Migani, A.; Neyman, K. Density Functional Modeling of the Interactions of Platinum Clusters with CeO_2 Nanoparticles of Different Size. *J. Phys. Chem. C* **2011**, *115*, 16081−16086.

DOI: 10.1021/acsami.5b00079
ACS Appl. Mater. Interfaces 2015, 7, 12671−12678

(48) Han, Y.; Liu, C. J.; Ge, Q. F. Interaction of Pt Clusters with the Anatase TiO_2(101) Surface: A First Principles Study. *J. Phys. Chem. B* **2006**, *110*, 7463−7472.
(49) Mulliken, R. S. Electronic Population Analysis on LCAO-MO Molecular Wave Functions 0.1. *J. Chem. Phys.* **1955**, *23*, 1833−1840.
(50) Roy, N.; Sohn, Y.; Pradhan, D. Synergy of Low-Energy (101) and High-Energy (001) TiO_2 Crystal Facets for Enhanced Photocatalysis. *ACS Nano* **2013**, *7*, 2532−2540.
(51) Gong, C.; Colombo, L.; Wallace, R. M.; Cho, K. The Unusual Mechanism of Partial Fermi Level Pinning at Metal-MoS_2 Interfaces. *Nano Lett.* **2014**, *14*, 1714−1720.
(52) Yoo, H.; Bae, C.; Yang, Y.; Lee, S.; Kim, M.; Kim, H.; Kim, Y.; Shin, H. Spatial Charge Separation in Asymmetric Structure of Au Nanoparticle on TiO_2 Nanotube by Light-Induced Surface Potential Imaging. *Nano Lett.* **2014**, *14*, 4413−4417.
(53) Murdoch, M.; Waterhouse, G. I. N.; Nadeem, M. A.; Metson, J. B.; Keane, M. A.; Howe, R. F.; Llorca, J.; Idriss, H. The Effect of Gold Loading and Particle Size on Photocatalytic Hydrogen Production from Ethanol over Au/TiO_2 Nanoparticles. *Nat. Chem.* **2011**, *3*, 489−492.
(54) Wang, W. N.; An, W. J.; Ramalingam, B.; Mukherjee, S.; Niedzwiedzki, D. M.; Gangopadhyay, S.; Biswas, P. Size and Structure Matter: Enhanced CO_2 Photoreduction Efficiency by Size-Resolved Ultrafine Pt Nanoparticles on TiO_2 Single Crystals. *J. Am. Chem. Soc.* **2012**, *134*, 11276−11281.
(55) Ma, Y.; Xu, Q.; Zong, X.; Wang, D. G.; Wu, G. P.; Wang, X.; Li, C. Photocatalytic H_2 Production on Pt/TiO_2-SO_4^{2-} with Tuned Surface-Phase Structures: Enhancing Activity and Reducing CO Formation. *Energy Environ. Sci.* **2012**, *5*, 6345−6351.
(56) Yu, J. G.; Qi, L. F.; Jaroniec, M. Hydrogen Production by Photocatalytic Water Splitting over Pt/TiO_2 Nanosheets with Exposed (001) Facets. *J. Phys. Chem. C* **2010**, *114*, 13118−13125.
(57) Pan, X. Y.; Xu, Y. J. Defect-Mediated Growth of Noble-Metal (Ag, Pt, and Pd) Nanoparticles on TiO_2 with Oxygen Vacancies for Photocatalytic Redox Reactions under Visible Light. *J. Phys. Chem. C* **2013**, *117*, 17996−18005.
(58) Long, R.; Mao, K. K.; Gong, M.; Zhou, S.; Hu, J. H.; Zhi, M.; You, Y.; Bai, S.; Jiang, J.; Zhang, Q.; Wu, X. J.; Xiong, Y. J. Tunable Oxygen Activation for Catalytic Organic Oxidation: Schottky Junction Versus Plasmonic Effects. *Angew. Chem., Int. Ed.* **2014**, *53*, 3205−3209.
(59) Hou, Y.; Li, X. Y.; Zou, X. J.; Quan, X.; Chen, G. C. Photoeletrocatalytic Activity of a Cu_2O-Loaded Self-Organized Highly Oriented TiO_2 Nanotube Array Electrode for 4-Chlorophenol Degradation. *Environ. Sci. Technol.* **2009**, *43*, 858−863.
(60) Sun, B.; Vorontsov, A. V.; Smirniotis, P. G. Role of Platinum Deposited on TiO_2 in Phenol Photocatalytic Oxidation. *Langmuir* **2003**, *19*, 3151−3156.
(61) Gan, S.; Liang, Y.; Baer, D. R.; Sievers, M. R.; Herman, G. S.; Peden, C. H. F. Effect of Platinum Nanocluster Size and Titania Surface Structure Upon CO Surface Chemistry on Platinum-Supported TiO_2 (110). *J. Phys. Chem. B* **2001**, *105*, 2412−2416.
(62) Tachikawa, T.; Yamashita, S.; Majima, T. Evidence for Crystal-Face-Dependent TiO_2 Photocatalysis from Single-Molecule Imaging and Kinetic Analysis. *J. Am. Chem. Soc.* **2011**, *133*, 7197−7204.
(63) Yang, L.; Luo, S.; Li, Y.; Xiao, Y.; Kang, Q.; Cai, Q. High Efficient Photocatalytic Degradation of *p*-Nitrophenol on a Unique Cu_2O/TiO_2 P-N Heterojunction Network Catalyst. *Environ. Sci. Technol.* **2010**, *44*, 7641−7646.
(64) Li, C.; Koenigsmann, C.; Ding, W.; Rudshteyn, B.; Yang, K. R.; Regan, K. P.; Konezny, S. J.; Batista, V. S.; Brudvig, G. W.; Schmuttenmaer, C. A.; Kim, J.-H. Facet-Dependent Photoelectrochemical Performance of TiO_2 Nanostructures: An Experimental and Computational Study. *J. Am. Chem. Soc.* **2015**, DOI: 10.1021/ja5111078.
(65) Jiang, B. J.; Tian, C. G.; Pan, Q. J.; Jiang, Z.; Wang, J. Q.; Yan, W. S.; Fu, H. G. Enhanced Photocatalytic Activity and Electron Transfer Mechanisms of Graphene/TiO_2 with Exposed {001} Facets. *J. Phys. Chem. C* **2011**, *115*, 23718−23725.

DOI: 10.1021/acsami.5b00079
ACS Appl. Mater. Interfaces 2015, 7, 12671−12678